Textures and Microstructures, 1989, Vol. 10, pp. 167–194
Reprints available directly from the publisher
Photocopying permitted by license only

Printed in the United Kingdom

Crystal Rotations Represented as Rodrigues Vectors

R. BECKER and S. PANCHANADEESWARAN
Alcoa Laboratories, Alcoa Center, PA 15069, U.S.A.

(Received May 16, 1988)

Rodrigues vectors are explored as a means of representing crystal orientation distributions. Relationships between the Rodrigues vectors and several more commonly utilized representations of rotations are presented. The restrictions which cubic material symmetry imposes on the Rodrigues space are examined and relationships for special equivalent configurations are developed. Common crystal orientation distributions are presented as Rodrigues vectors and compared to the more standard representations in terms of pole figures and Euler angles. Applications of the Rodrigues space for illustrating misorientations between neighboring grains are also discussed.

KEY WORDS: Rodrigues space, Euler angles, ODF representation.

INTRODUCTION

The Crystallite Orientation Distribution Function (CODF) is widely used to represent the relative orientation of individual crystallites within a sample to a set of sample axes. Since the CODF is computed in terms of spherical harmonics expressed as a function of the three Euler angles, a natural choice of variables with which to represent the distribution of orientations, or texture, are the Euler angles. In most cases, these three angles are uniquely defined by the rotation of the sample axes to the orientation of the crystal axes. A drawback to the use of Euler angles, however, is that it is difficult to visualize rotations when given the angles. The representation does not have a simple physical interpretation and identification of

particular orientations involves comparison with calculated standards. A more easily interpreted representation of rotations would be desirable.

An extensive discussion of various representations of rotations is given by Altmann (1986) and Hansen *et al.* (1978). While several of these are readily handled mathematically, rotations expressed as axis-angle pairs are both conceptually and mathematically simple. This representation follows from a theorem by Euler. Euler (1775) has shown that the rotation of a rigid body from a reference orientation can be characterized uniquely by an axis of rotation, given in terms of its direction cosines $\mathbf{c}$ (a unit vector), and the angle of rotation about that axis, ω. The representation is unique if ω is within a range of rotations which is determined by the symmetry of the material.

Hence, an alternative method of representing crystallographic orientations within a sample would be in terms of an axis of rotation and a simple function of the rotation angle.

$$\Lambda = \mathbf{c}f(\omega). \tag{1}$$

The choice of an appropriate form for $f(\omega)$ is discussed by Frank (1986) who considers several functional forms. A relation that stands out because of its algebraic significance and geometric simplicity is $f(\omega) = \tan(\omega/2)$. The representation of rotations in this space, for materials with cubic symmetry, is examined by Frank (1986). Here his findings are reproduced by a more direct method. Details of the calculations are included for completeness.

Calculated textures from several simulated deformation histories are presented as pole figures, CODFs in terms of Euler angles and as vectors in the space defined above. In addition, the measured misorientation of neighboring grains within a specimen are shown to illustrate an alternative application of the axis-angle pair representation. Several advantages and disadvantages of this representation compared to the standard CODF in terms of Euler angles are discussed.

RODRIGUES PARAMETERS

The origin of (1) with $f(\omega) = \tan(\omega/2)$ can be attributed to Rodrigues (1840). He determined the composition of two rotations,

expressed in terms of their axes and angles of rotation, and obtained the axis and angle of the resultant rotation. To achieve this, the rotation is expressed in terms of 4 parameters,

$$\rho = \cos(\omega/2), \quad \lambda = c_1 \sin(\omega/2), \quad \mu = c_2 \sin(\omega/2), \quad \nu = c_3 \sin(\omega/2), \tag{2}$$

known, perhaps inappropriately,† as the Euler parameters or Euler–Rodrigues parameters. While there are 4 parameters, in general only 3 are needed to characterize a rotation; the condition

$$\rho^2 + \lambda^2 + \mu^2 + \nu^2 = 1, \tag{3}$$

resulting from $\mathbf{c}$ being a unit vector, provides an additional restriction on the parameters.

These parameters can be combined to represent rotations in terms of (Korn and Korn, 1968):

a) Rotation matrix‡

$$A = \begin{pmatrix} \lambda^2 - \mu^2 - \nu^2 + \rho^2 & 2(\lambda\mu - \nu\rho) & 2(\nu\lambda + \mu\rho) \\ 2(\lambda\mu + \nu\rho) & \mu^2 - \nu^2 - \lambda^2 + \rho^2 & 2(\mu\nu - \lambda\rho) \\ 2(\nu\lambda - \mu\rho) & 2(\mu\nu + \lambda\rho) & \nu^2 - \lambda^2 - \mu^2 + \rho^2 \end{pmatrix}. \tag{4}$$

b) Euler angles

$$\begin{aligned} \psi &= \tan^{-1}(\nu/\rho) - \tan^{-1}(\lambda/\mu) \\ \theta &= 2\tan^{-1}\left(\frac{\lambda^2 + \mu^2}{\nu^2 + \rho^2}\right)^{1/2} \\ \phi &= \tan^{-1}(\nu/\rho) + \tan^{-1}(\lambda/\mu). \end{aligned} \tag{5}$$

c) Rodrigues vector

$$\mathbf{R} = \frac{\lambda}{\rho}\mathbf{e}_1 + \frac{\mu}{\rho}\mathbf{e}_2 + \frac{\nu}{\rho}\mathbf{e}_3, \tag{6}$$

where $\mathbf{e}_i$ are rectangular Cartesian base vectors.

† Although the concept of the axis-angle pair was proposed by Euler (1775), the key feature here is the use of the half angle, which is due to Rodrigues (1840).

‡ Here the rotation matrix describes the rotation of a body to a new configuration in terms of the original unrotated axes. This is equal to the transpose of the matrix often cited in Material Science literature (e.g. Roe, 1965), which is essentially a coordinate transformation relating a vector in the original coordinate system to the same vector in the rotated system.

d) Caley–Klein parameters (complex numbers)

$$a = \rho + iv, \qquad b = \mu + i\lambda. \tag{7}$$

e) Quaternions

$$\Phi = \rho + i\lambda + j\mu + kv. \tag{8}$$

The inverse relationships for (4) and (5) allow determination of the Euler–Rodrigues parameters in terms of more conventional representations. The direction cosines of the rotation axis, c_i, and the rotation angle, ω, can be obtained from a rotation matrix, A, by:

$$\cos\omega = \tfrac{1}{2}[\mathrm{Tr}(A) - 1],$$
$$c_1 = \frac{A_{32} - A_{23}}{2\sin\omega}, \qquad c_2 = \frac{A_{13} - A_{31}}{2\sin\omega}, \qquad c_3 = \frac{A_{21} - A_{12}}{2\sin\omega}, \tag{9}$$

where $\mathrm{Tr}(A)$ indicates the trace of matrix A. The parameters in (2) can also be expressed in terms of the Euler angles, (ψ, θ, ϕ), as

$$\rho = \cos\frac{\psi + \phi}{2}\cos\frac{\theta}{2}, \qquad \lambda = \sin\frac{\phi - \psi}{2}\sin\frac{\theta}{2},$$
$$\mu = \cos\frac{\phi - \psi}{2}\sin\frac{\theta}{2}, \qquad v = \sin\frac{\psi + \phi}{2}\cos\frac{\theta}{2}. \tag{10}$$

Combinations of two rotations to obtain a composite rotation of the same form can be achieved directly for each of the above representations except the Euler angles. For example, two rotation matrices, A_{ij} and B_{jk}, can be multiplied directly by standard matrix algebra to determine the composite rotation;

$$C_{ik} = \sum_{j=1}^{3} A_{ij}B_{jk}. \tag{11}$$

The Rodrigues vector, $\mathbf{R}_c$, resulting from two successive rotations, $\mathbf{R}_a$ followed by $\mathbf{R}_b$, is obtained by standard vector operations;

$$\mathbf{r}_c = \frac{\mathbf{R}_a + \mathbf{R}_b - (\mathbf{R}_a \times \mathbf{R}_b)}{1 - \mathbf{R}_a \cdot \mathbf{R}_b}. \tag{12}$$

The Caley–Klein parameters can be combined in various ways to represent rotations. They are commonly associated with Pauli spin matrices for quantum mechanics applications. In a simpler form,

however, they can be viewed as a mapping which rotates stereographic projections of one configuration, U, to another, U'.

$$U' = \frac{aU - b^*}{bU + a^*}, \tag{13}$$

where a^* and b^* are the complex conjugates of a and b, respectively. Frank (1986) uses these parameters to find the boundaries of the Rodrigues space imposed by cubic crystal symmetry, but a more direct approach involving quaternions is used here.

Quaternion algebra is not as widely known as matrix or vector algebra, so a few of the basic rules are presented below. First, it should be mentioned that a quaternion is a mapping and that the quaternion in (8) with the parameters given by (2) is a pure rotation, $|\Phi| = 1$. For a more general quaternion, each of the terms would be multiplied by a constant, allowing for expansion in addition to rotation. The combination of rotations involves successive mappings and therefore the product of quaternions. The product rules for the three quaternion units, i, j and k, are

$$\begin{gathered} ii = jj = kk = -1, \\ ij = -ji = k, \qquad jk = -kj = i, \qquad ki = -ik = j, \end{gathered} \tag{14}$$

from which it can be seen that multiplication is noncommutative. It is interesting to note that if $\mu = \nu = 0$, the quaternion behaves as a complex variable mapping in 2-dimensional space. Using the above product rules, the product of 2 quaternions, Φ_a followed by Φ_b, yields a third quaternion, Φ_c.

$$\begin{aligned} \Phi_c = \rho_c + i\lambda_c + j\mu_c + k\nu_c = \Phi_b\Phi_a = {} & \rho_b\rho_a - \lambda_b\lambda_a - \mu_b\mu_a - \nu_b\nu_a \\ & + i(\lambda_b\rho_a + \rho_b\lambda_a - \nu_b\mu_a + \mu_b\nu_a) \\ & + j(\mu_b\rho_a + \nu_b\lambda_a + \rho_b\mu_a - \lambda_b\nu_a) \\ & + k(\nu_b\rho_a - \mu_b\lambda_a + \lambda_b\mu_a + \rho_b\nu_a). \end{aligned} \tag{15}$$

Defining $\Phi^* \equiv \rho - i\lambda - j\mu - k\nu$, then $\Phi\Phi^* = \Phi^*\Phi \equiv |\Phi|^2$. For the pure rotations considered here, $|\Phi| = 1$. The inverse rotation, $\Phi^*/|\Phi|^2$, can be viewed as a rotation about the same axis with a negative angle of rotation or as the same angular rotation with the

direction cosines equal to the negative of those for Φ. Here, all rotations will be assumed $0 \leq \omega < \pi$ so that the trigonometric functions always evaluate as positive.

MATERIAL SYMMETRY

For an arbitrary body, representation of rotations by Rodrigues vectors is unique when $\omega < \pi$, with the space being unbounded for $\omega = \pi$. For materials which exhibit symmetry, however, the rotations can be defined within a finite subspace. Here, the bounds of the space are determined for materials with cubic symmetry. Consistent with the adopted convention that all rotation angles be positive, the subspace contains the origin and the bounds are orthotropic with respect to the Cartesian coordinate axes, for cubic materials.

The bounds of the subspace are determined by searching for rotations, with different rotation axes but the same rotation angle, which give equivalent configurations. For example, a cube initially aligned with the coordinate axes, X_i, rotated 45° about the ${}^{+}X_3$ axis gives the same configuration as a 45° rotation about the ${}^{-}X_3$ axis, Figure 1a. To determine the boundaries that the symmetry imposes on the space, consider a cube with edges initially parallel to the coordinate directions which will be rotated to a generic orientation Φ with respect to the coordinate axes, Figure 1b. Rotation of the cube 90° about the cube's x_3 axis, $\Phi' = 1/\sqrt{2} + k(1/\sqrt{2})$, *prior* to the rotation, Φ, will give an equivalent orientation,

$$\Phi'' = \Phi\Phi' = \frac{1}{\sqrt{2}}(\rho - \nu) + i\frac{1}{\sqrt{2}}(\lambda + \mu) + j\frac{1}{\sqrt{2}}(\mu - \lambda) + k\frac{1}{\sqrt{2}}(\rho + \nu). \tag{16}$$

With the angles of rotation for Φ and Φ'' set equal to determine the location of the symmetry boundary,

$$\rho'' = \frac{1}{\sqrt{2}}(\rho - \nu) = \rho, \tag{17}$$

which gives;

$$\nu = (1 - \sqrt{2})\rho = c_3 \sin(\omega/2). \tag{18}$$

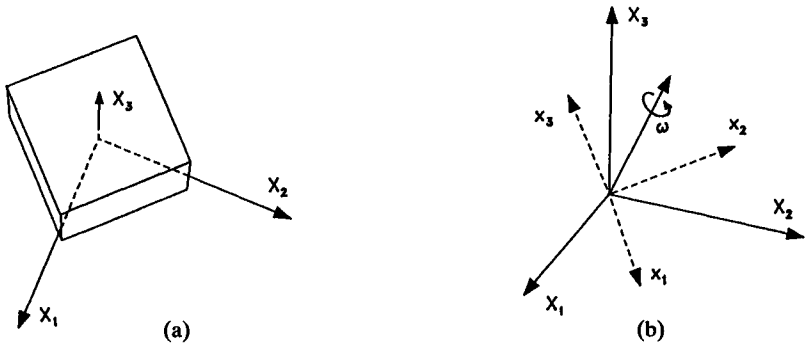

Figure 1 (a) Rotation of a cube about X_3, (b) Rotation of local coordinate axes about a rotation axis.

Since the angle is positive, this condition defines a surface for which $c_3 < 0$. Solving for $\sin(\omega/2)$, substituting in (2) and using the resulting expressions for the Euler–Rodrigues parameters in (16) yields:

$$\Phi'' = \rho + i(c_1 + c_2)\frac{1-\sqrt{2}}{c_3\sqrt{2}}\rho + j(c_2 - c_1)\frac{1-\sqrt{2}}{c_3\sqrt{2}}\rho + k(\sqrt{2}-1)\rho. \tag{19}$$

Applying the condition that $\rho''^2 + \lambda''^2 + \mu''^2 + \nu''^2 = 1$,

$$\rho = \cos(\omega/2) = \frac{-c_3}{[c_3^2 + (\sqrt{2}-1)^2]^{1/2}}, \tag{20}$$

where the minus sign is chosen to retain $\rho > 0$. Thus,

$$\sin(\omega/2) = \frac{1-\sqrt{2}}{c_3}\rho = \frac{\sqrt{2}-1}{[c_3^2 + (\sqrt{2}-1)^2]^{1/2}}, \tag{21}$$

and

$$\Phi'' = \cos(\omega/2) + i\frac{1}{\sqrt{2}}(c_1 + c_2)\sin(\omega/2)$$

$$+ j\frac{1}{\sqrt{2}}(c_2 - c_1)\sin(\omega/2) - kc_3\sin(\omega/2). \tag{22}$$

Table 1 Equivalent locations

Face direction	c_1''	c_2''	c_3''
(−1, 0, 0)	$-c_1$	$\frac{1}{\sqrt{2}}(c_2+c_3)$	$\frac{1}{\sqrt{2}}(c_3-c_2)$
(0, −1, 0)	$\frac{1}{\sqrt{2}}(c_1-c_3)$	$-c_2$	$\frac{1}{\sqrt{2}}(c_3+c_1)$
(0, 0, −1)	$\frac{1}{\sqrt{2}}(c_1+c_2)$	$\frac{1}{\sqrt{2}}(c_2-c_1)$	$-c_3$
(−1, −1, −1)	$-c_3$	$-c_1$	$-c_2$
(−1, 1, 1)	c_3	c_1	$-c_2$
(1, −1, 1)	$-c_3$	c_1	c_2
(1, 1, −1)	c_3	$-c_1$	c_2

Hence, for this particular symmetry rotation about the x_3 axis,

$$c_1'' = (c_1 + c_2)/\sqrt{2} \qquad c_2'' = (c_2 - c_1)/\sqrt{2} \qquad c_3'' = -c_3, \tag{23}$$

which define the direction cosines of the equivalent rotation vector. Furthermore, $\tan(\omega/2) = -(\sqrt{2}-1)/c_3$ so that, for the material with cubic symmetry, the extent of the Rodrigues space in the X_3 direction is $(1-\sqrt{2})$ and $(\sqrt{2}-1)$. This defines two planes perpendicular to the X_3 axis as bounds to the subspace. Similar calculations yield equivalent relations for boundaries of the space perpendicular to the other coordinate axes. These are summarized by the first three entries in Table 1.

In addition to these boundaries, other boundaries are found by composite rotations such as 90° about the x_1 axis followed by a 90° rotation about the x_3 axis; $\Phi' = \frac{1}{2} + i\frac{1}{2} + j\frac{1}{2} + k\frac{1}{2}$. This is a 60° rotation about a cube diagonal. Manipulations similar to those above yield:

$$\rho = \cos(\omega/2) = -(\lambda + \mu + \nu) = -(c_1 + c_2 + c_3)\sin(\omega/2), \tag{24}$$

where $(c_1 + c_2 + c_3) < 0$. Applying the condition that $|\Phi''| = 1$,

$$\cos(\omega/2) = \frac{-(c_1+c_2+c_3)}{[1+(c_1+c_2+c_3)^2]^{1/2}} \qquad \sin(\omega/2) = \frac{1}{[1+(c_1+c_2+c_3)^2]^{1/2}}. \tag{25}$$

The equivalent rotation is

$$\Phi'' = \cos(\omega/2) - ic_3\sin(\omega/2) - jc_1\sin(\omega/2) - kc_2\sin(\omega/2), \tag{26}$$

and

$$c_1'' = -c_3 \qquad c_2'' = -c_1 \qquad c_3'' = -c_2. \tag{27}$$

The limiting surface in Rodrigues space determined by this symmetry condition is found by substituting (25) into (2) and using the resulting parameters in (6). The vectors define the surface at

$$\mathbf{R} = \frac{-c_3}{c_1 + c_2 + c_3}\mathbf{e}_1 + \frac{-c_1}{c_1 + c_2 + c_3}\mathbf{e}_2 + \frac{-c_2}{c_1 + c_2 + c_3}\mathbf{e}_3. \tag{28}$$

These coordinates satisfy the equation for a plane, $aX_1 + bX_2 + cX_3 = d$, with its normal in the $(-1, -1, -1)$ direction. The angle for symmetry rotations about the cube diagonal, $c_1 = c_2 = c_3 = -1/\sqrt{3}$, is then $\omega = 2\tan^{-1}(1/\sqrt{3}) = 60°$. Additional planes are found at other corners of the space. These are listed in Table 1 with their equivalent material symmetry orientations.

For a material with cubic symmetry, all rotations are uniquely represented within a cube with truncated corners defined by the inner envelope of the surfaces described above, Figure 2. Rodrigues vectors falling outside of this surface have an equivalent rotation inside the surface. For any set of equivalent symmetry rotations, the one with the smallest angle, ω, lies within the surface. Points on the surface represent rotations which have an equivalent rotation on another face. Given a rotation axis, $\mathbf{c}$, the Rodrigues vector increases in length as the angle of rotation about that axis increases. When the vector reaches one of the bounding surfaces, the rotation, which had been represented by Φ, has an equivalent representation in Φ'', with axis $\mathbf{c}''$. The point corresponding to Φ'' is located by referring to the entry in Table 1 corresponding to the face which the

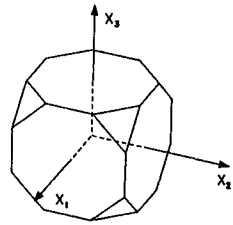

Figure 2 Planar bounds of the subspace set by consideration of cubic material symmetry.

vector has exited. Relations for the faces not listed in the table can easily be obtained by inverting the relation between $\mathbf{c}$ and $\mathbf{c}''$. On the bounding surfaces, the angle of rotation, ω, is the same for Φ and Φ''.

Similarly, a texture fiber leaving the space with direction cosines $\mathbf{c}$ will reenter the subspace on another face where the Rodrigues vector has direction cosines $\mathbf{c}''$. As indicated above, these surfaces are identified in Table 1 by their outward normal direction. The direction cosines of the Rodrigues vector on the face which the fiber exits are used to identify the direction cosines of the equivalent rotation where the fiber will reenter the subspace.

Calculating the Rodrigues vectors for a material with cubic symmetry requires determination of which of the 24 equivalent rotations places the vector within the subspace. This is computationally efficient when done either in terms of rotation matrices or quaternions, since only (9a) or ρ_c from (15), respectively, needs to be determined for all 24 symmetry rotations. For rotation matrices, this involves only 4 addition operations per symmetry rotation. The number of operations for quaternions ranges from a simple assignment statement to a multiplication and 4 additions for each of the 24 rotations. The symmetry rotation which yields the greatest result for (9a) or for ρ_c from (15) will give the smallest rotation angle. With the rotation determined, the remaining parameters are only calculated for the selected rotation.

TEXTURE REPRESENTATIONS

A distribution of rotations characterized by Rodrigues vectors resides in a 3-dimensional space. If the rotations of crystallites are represented by discrete points at the ends of the vectors, a line drawn from the center of the space through a point is the rotation axis for that crystallite. The amount of rotation about the axis is related to the distance from the center by $d = \tan(\omega/2)$. The crystal is rotated from its reference configuration, where the crystal axes are coincident with the subspace axes, to its present orientation. This provides a simple physical representation of rotations.

Several techniques are available for examining the spatial distribution of rotations in Rodrigues space. In addition to viewing the

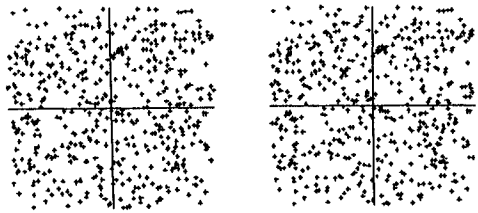

Figure 3 Stereographic pair showing a random distribution of rotations represented by Rodrigues vectors.

space from various projections and by stereoscopic images, Figure 3, video displays which can rotate the space in real time provide an excellent means for visualizing the 3-dimensional structure. Such tools are invaluable for assessing the pattern of rotation distributions in Rodrigues space.

The rotations must be presented in 2-dimensions for printed presentation. Here, the space is sectioned into finite width slices perpendicular to an axis. The ends of the vectors are indicated as points with all points within a slice being plotted in one frame. The frames are labelled by the specimen coordinate axes and the sections are identified by the normalized distance from the center to the midplane of the slice, with the faces being unity. This is illustrated by Figure 4 which shows 500 random rotations. In this space, random rotations will appear as nearly uniform coverage at the center and the points will be somewhat more diffuse at the boundaries. This appears to be the case in Figure 4, but here there are too few points to give a good feel for the density distribution.

Texture evolution with deformation was simulated using the rate dependent Taylor-type polycrystal model of Asaro and Needleman (1985). The initial grain distribution, represented by Figure 4, was subjected to various deformation histories. Details of the model and properties used are not important in this context.

Figure 5a shows the Rodrigues space representation of the distribution of grain orientations following uniaxial compression to 25% of its original height. The space is sectioned perpendicular to the compression axis, X_2. The texture fibers form as shells around the ideal $\langle 110 \rangle$ fiber which is shown in Figure 5b. The ideal $\langle 110 \rangle$ fibers run basically in the direction of the compression axis along

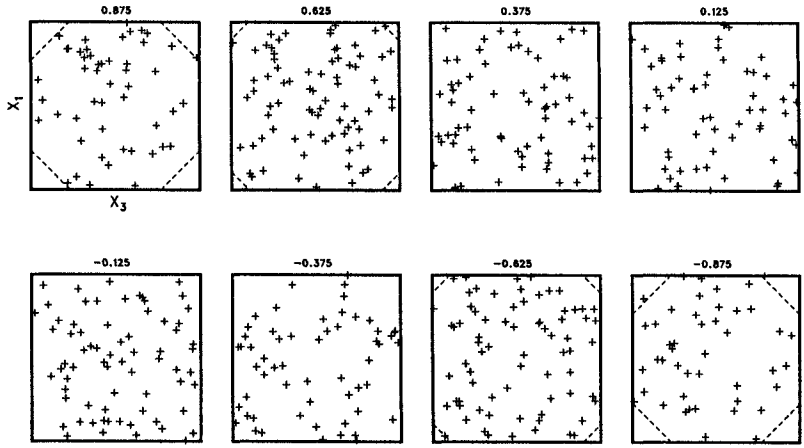

Figure 4 Random distribution of rotations shown as sections of the Rodrigues space.

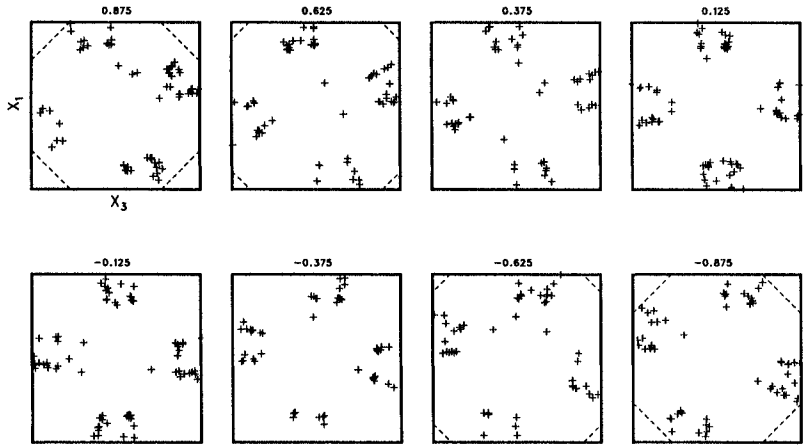

Figure 5(a) Rodrigues space representation of grain orientations following uniaxial compression along X_2.

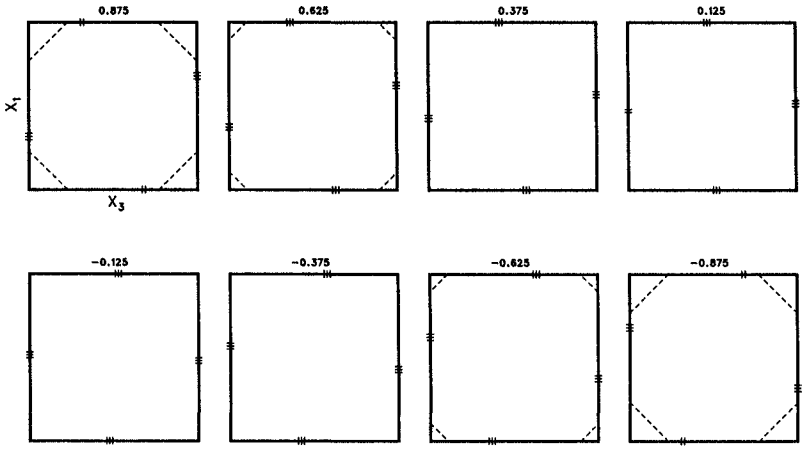

Figure 5(b) Ideal ⟨110⟩ fiber texture in Rodrigues space.

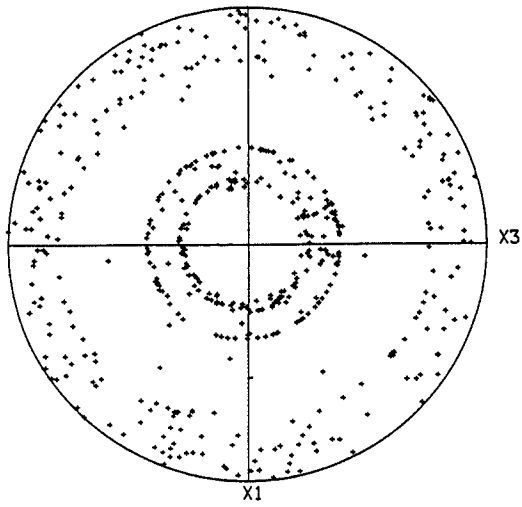

Figure 5(c) (111) pole figure of compression texture.

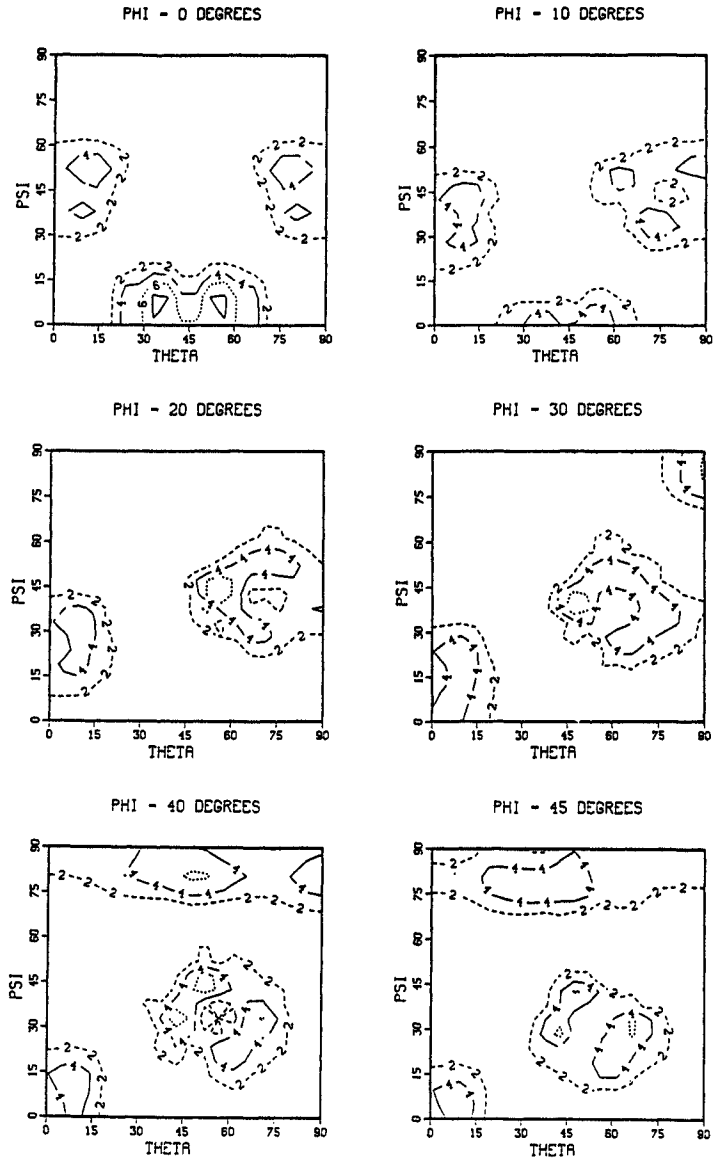

Figure 5(d) Compression texture shown as CODF using Euler angles.

the boundaries of the subspace with a 45° counterclockwise twist from -1 to 1. Figure 5c shows the same orientation distribution in the form of a (111) pole figure with the compression axis, X_2, normal to the plane of the paper. A strong fiber component near $\langle 110 \rangle$ may be seen as two rings on the pole figure. In Figure 5d, the crystallite orientation distribution function (CODF) is plotted as a function of the Euler angles ψ, θ and ϕ in Roe's (1965) notation. This is obtained by expanding each ideal orientation in generalized spherical harmonics. The CODF is represented in the form of contour plots in constant ϕ cross sections. In order to show the fiber texture, however, the sample coordinates are rotated such that X_1 is the compression axis. Two variants of $\langle 110 \rangle$ fiber may be observed.

The calculated grain orientation distribution for uniaxial tension is shown in Figure 6. Figure 6a is the distribution of rotations in Rodrigues space, sectioned parallel to the tensile axis (X_2). Two developing fiber textures are shown. The weaker fiber is $\langle 100 \rangle$ type that lies along a line through the center of each frame, parallel to the tensile axis. The stronger texture is near an ideal $\langle 111 \rangle$ fiber, shown in Figure 6b. A (111) pole figure and a representation in

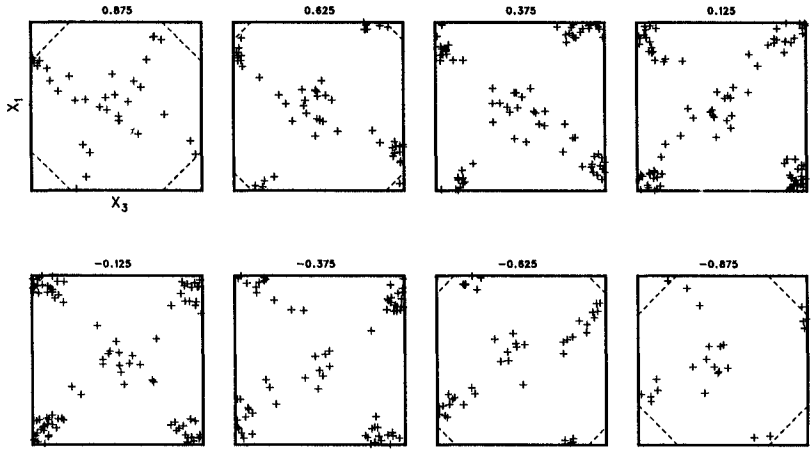

Figure 6(a) Rodrigues space representation of grain orientations following uniaxial tension along X_2.

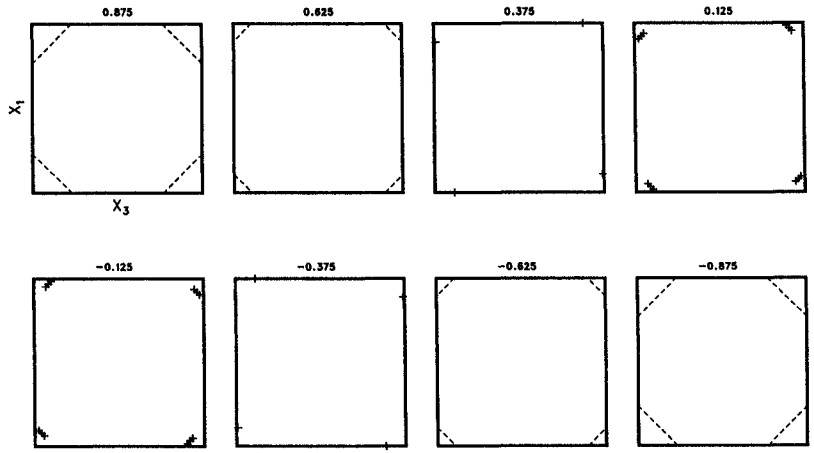

Figure 6(b) Ideal ⟨111⟩ fiber texture in Rodrigues space.

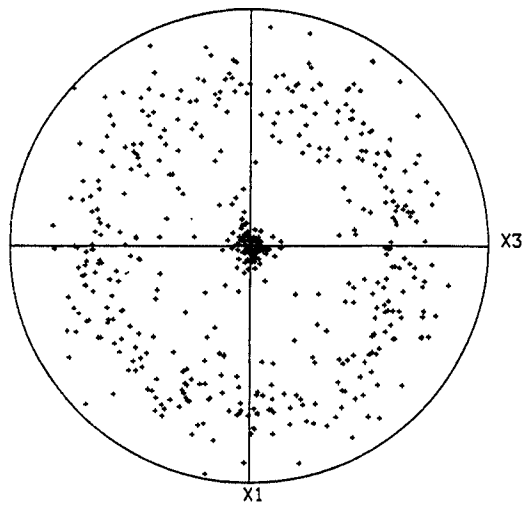

Figure 6(c) (111) pole figure of tension texture.

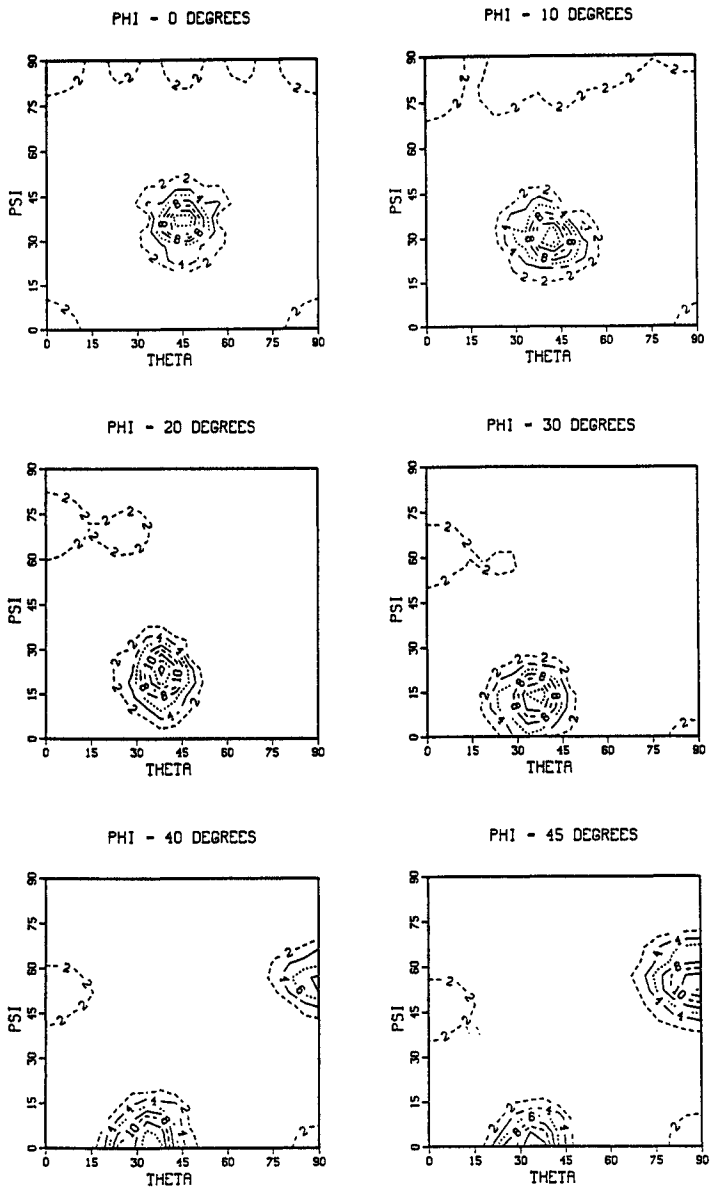

Figure 6(d) Tension texture shown as CODF using Euler angles.

Euler space are shown in Figures 6c and 6d, respectively. The strong ⟨111⟩ fiber and a mild ⟨100⟩ fiber are seen here also.

Figure 7a shows a distribution of grains about an ideal rolling texture (Hirsch *et al.*, 1987). This texture is generated by mixing several Gaussian distributions around individual rolling components. The space is sectioned perpendicular to the rolling direction and the normal and transverse directions are labelled. Ideal components along a fiber from the Brass orientation (labelled 1) through Copper (6) are plotted in Figure 7b and listed in terms of Euler angles and Rodrigues vectors in Table 2. These are also indicated on the (111) pole figure, Figure 7c. Specimen symmetry provides for three additional fibers with equivalent characteristics. Figure 7d shows the CODF in the Euler angle representation.

The next example considered is uniaxial compression of a sample made from an extruded rectangular bar. The compression samples were prepared with the compression axis, X_2, parallel to the short transverse direction in the extrusion geometry. Because the starting

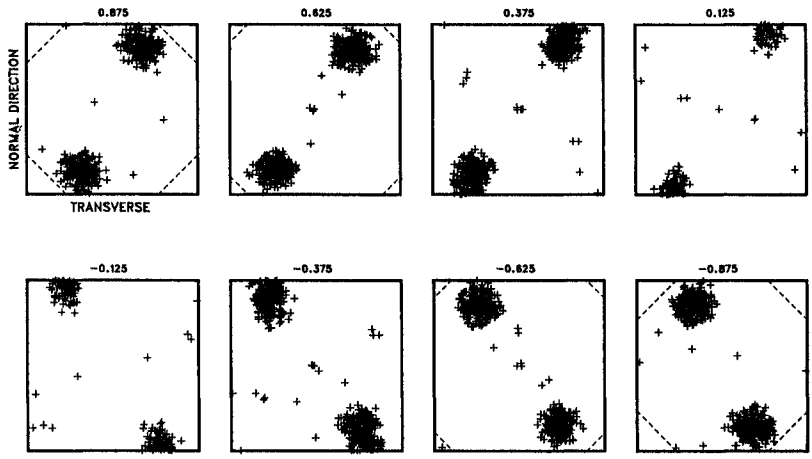

Figure 7 Simulated rolling texture generated by allowing a 5° spread along a skelton line. (a) Representation in Rodrigues space.

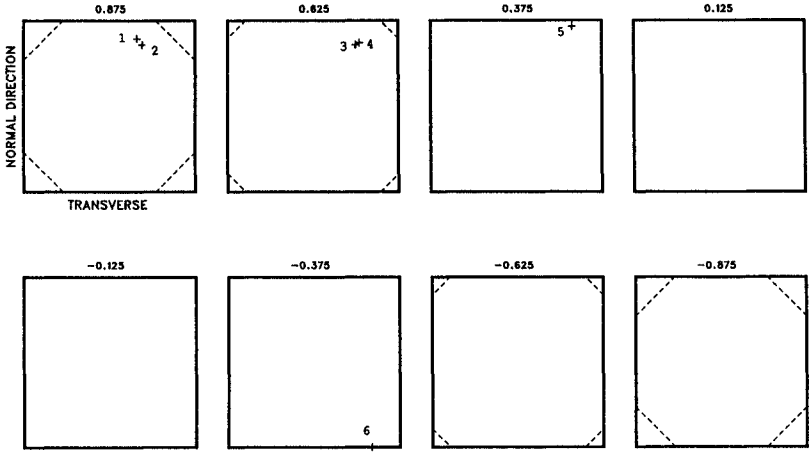

(b)

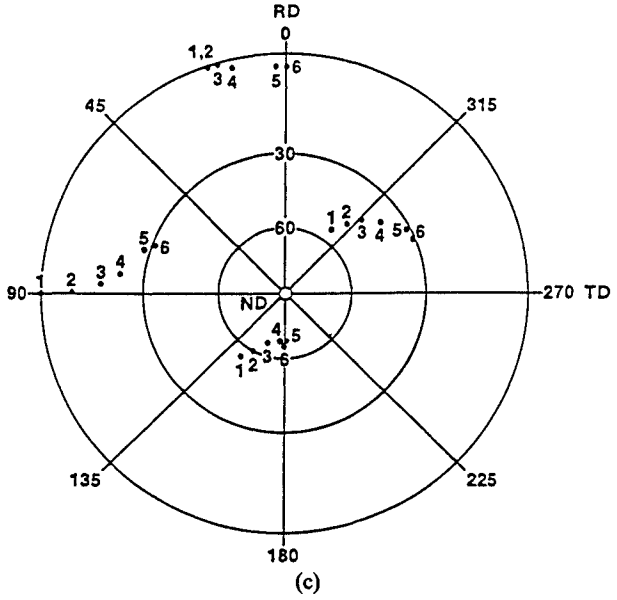

(c)

Figure 7(b) and (c) Major components of rolling texture skelton as Rodrigues vectors and as a (111) pole figure (from Fricke and Przystupa, 1988).

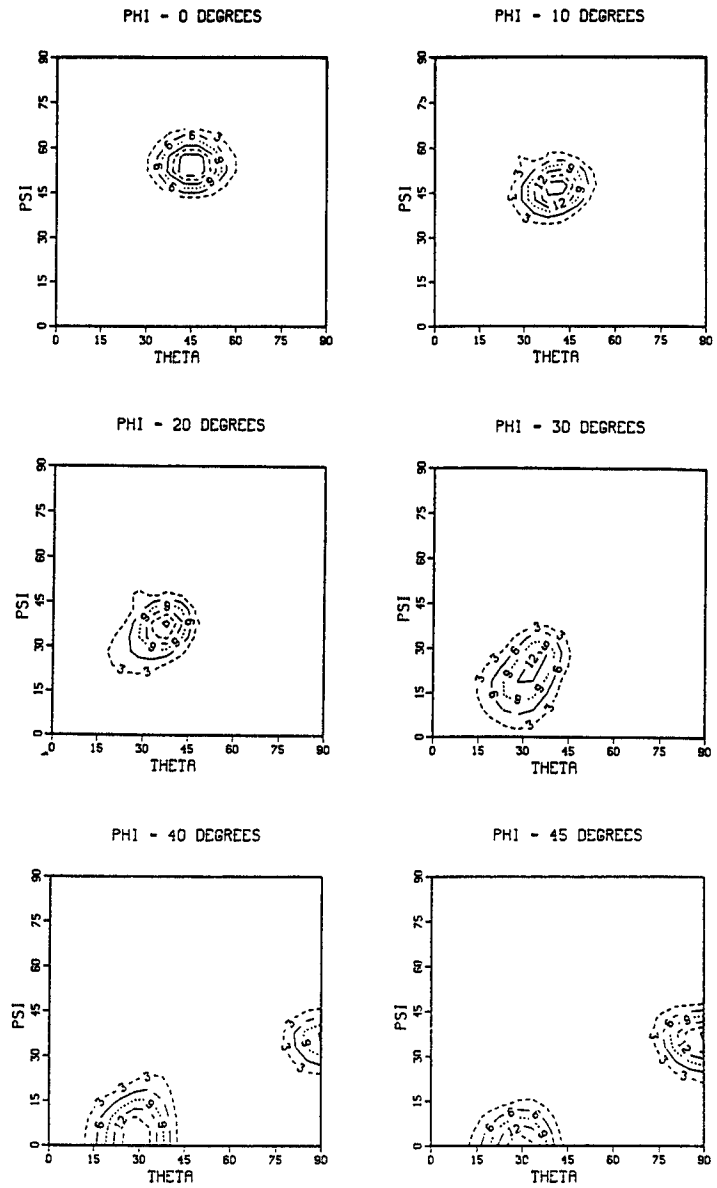

Figure 7(d) Simulated rolling texture as a CODF in terms of Euler angles.

Table 2 Ideal rolling texture components

Component	ψ	θ	ϕ	R_1	R_2	R_3
1	54	45	0	0.4142	0.1346	0.3249
2	47	38	10	0.3214	0.1602	0.2962
3	37	37	20	0.2805	0.2076	0.2962
4	26	33	30	0.2112	0.2265	0.3057
5	8	32	40	0.1489	0.2686	0.3839
6	0	31	45	−0.1149	0.2773	−0.4142

material has a strong texture, the deformation is not axisymmetric. The sample, which was originally circular in cross section, transformed into an oval shape with predominant elongation in the extrusion direction, X_1. The details of the experimental procedure will be described in a separate report. The final texture, as predicted by the polycrystal deformation model, has a fairly strong rolling texture due to the anisotropic nature of the deformation. As may be observed in Figure 8, the model predicts the development of "rolling like" texture in the original extrusion direction, X_1. It may also be noticed that, unlike the case of compression with random starting texture (Figure 5d) where uniform distribution of planes containing ⟨110⟩ fiber is observed, here the fiber is clustered near (110)[001] or the "Goss" orientation.

The final texture after 75% reduction is shown in Figure 8a, sectioned parallel to the X_1 direction with X_2 being the compression axis (also the short transverse direction). The similarity between Figure 8a and the ideal rolling texture of Figure 7b can be seen. In comparing these two figures, however, it must be remembered that the compression axis is labelled "X_2" in Figure 8a and is labelled "normal direction" in Figure 7a. The (111) pole figure and a CODF in Euler angle space are shown in Figures 8b and 8c, respectively. In Figure 8c, the CODF is plotted in a transformed coordinate system with the sample X_3 axis parallel to the compression axis and X_1 being the original extrusion direction. This was done to emphasize the predominantly rolling like texture that was predicted by the polycrystal model. The "Goss" texture may be seen in zero degree ϕ cross sections at $\psi = 90$ and $\theta = 45$. In Rodrigues space the "Goss" texture is in the center of the 0.875 and −0.875 cross sections of Figure 8a.

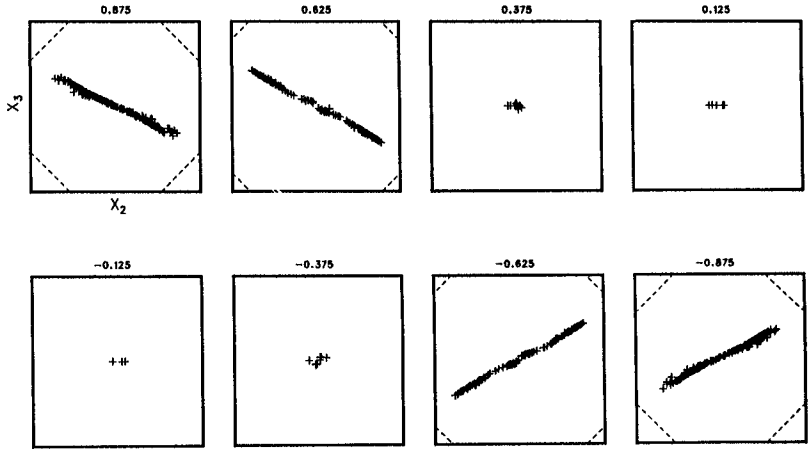

(a)

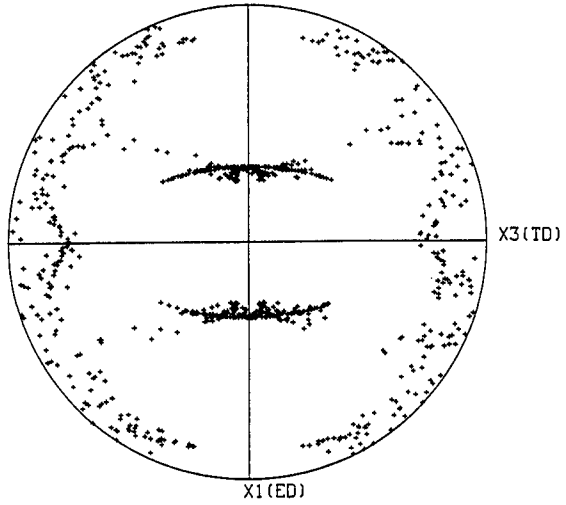

(b)

Figure 8 Rodrigues space representation (a) of grain orientations for extrusion followed by uniaxial compression; (b) (111) pole figure of uniaxial compression on previously extruded material.

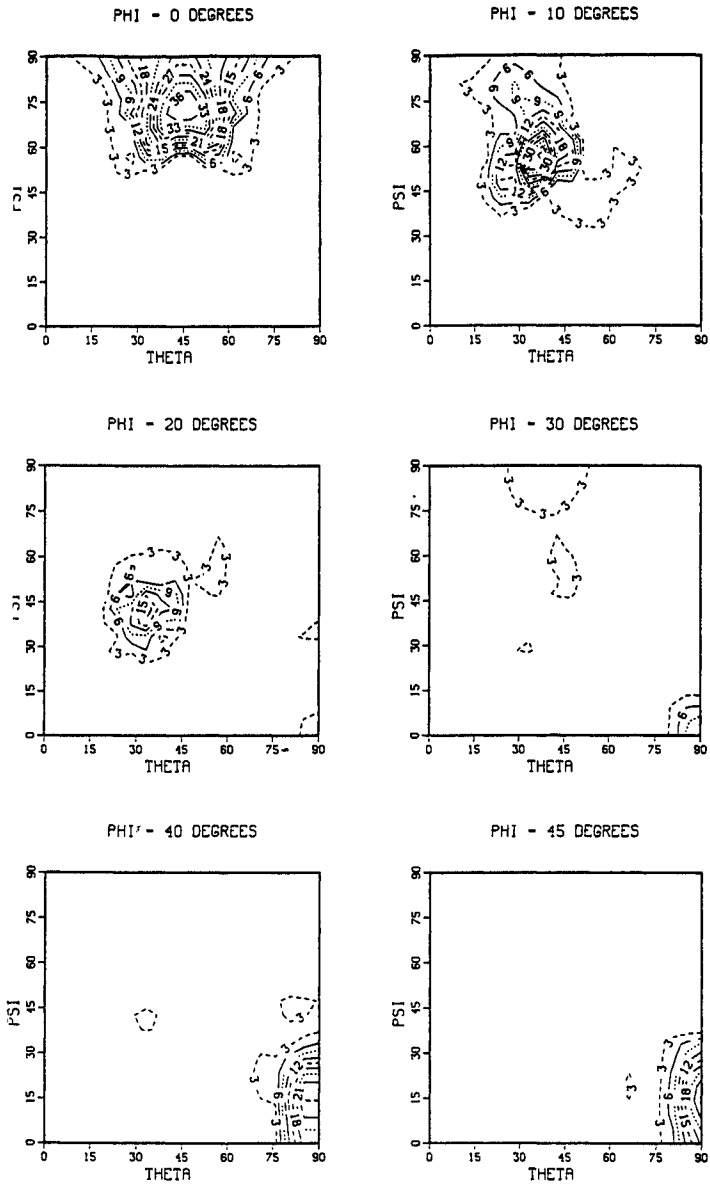

Figure 8(c) Euler angle space for extrusion followed by uniaxial compression.

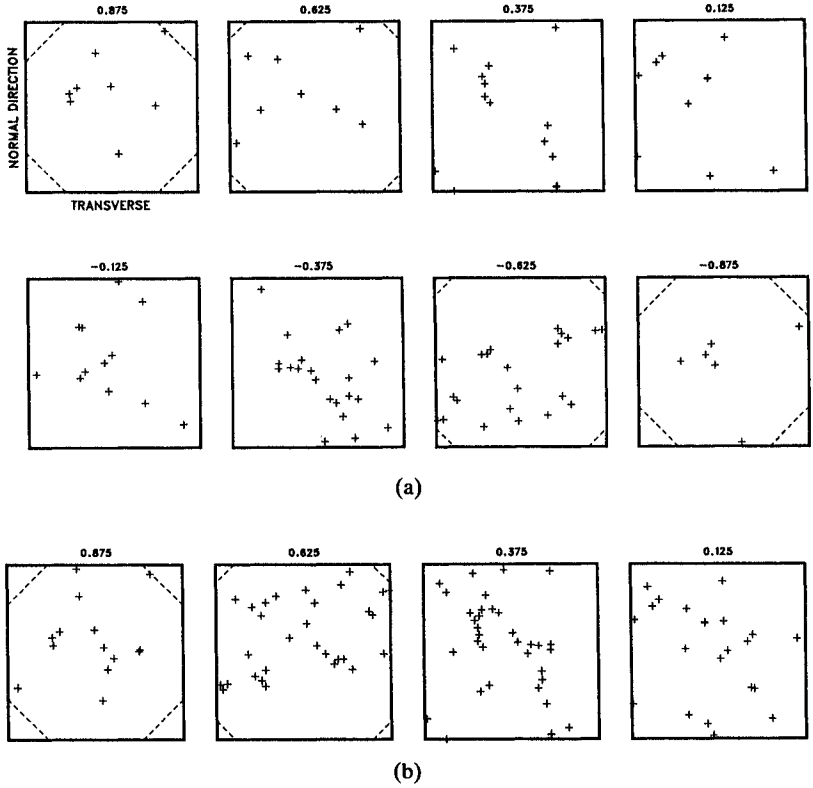

Figure 9 Measured distribution of grain orientations from an annealed sheet (a) and rotational misorientation of neighboring grains (b).

In order to emphasize a compression fiber parallel to the X_2 axis, the CODF would have to be reconstructed in another coordinate system. On the other hand, the representation in Rodrigues space is fixed for a given grain distribution, and in order to view it from a different orientation it is merely sectioned along a different axis. The description of orientation in Euler angle space is, therefore, at a disadvantage because it does not have a direct contact with physical space through the laboratory or sample coordinte system. A different 3-dimensional representation must be constructed depending on which of the coordinate axes is designated X_3. Three

dimensional texture representation in Rodrigues space eliminates this problem.

Rotation of a crystallite to its present orientation (from a reference orientation which is fixed with respect to the specimen axes) defines the rotation axis in terms of the sample coordinates. Hence, the vectors in Rodrigues space are fixed by the specimen and are not an artifact of the representation. If the coordinates of the Rodrigues space are aligned with the specimen axes, sample symmetries will also show up as symmetries in Rodrigues space. This symmetry is evident in the simulated rolling texture of Figure 7a. Likewise, any asymmetry in the distribution of grain orientations manifests itself as an asymmetry in Rodrigues space. Figure 9a shows a distribution of rotations measured from annealed sheet material. The orientations were determined for individual grains by examining the Kikuchi patterns created by backscatter electrons in an SEM (Venables and Harland, 1973; Dingley, 1987). While the number of grains is small, the asymmetry of the orientation distribution is evident.

A significant advantage of the Rodrigues representation may be realized in analysis of nonconventional features such as representing the misorientation between neighboring grains. Here the symmetry of the space is a particular asset. Using the technique described above for measuring individual grain orientations, it is also possible to keep track of which grains are neighbors. Consider the rotation of two neighboring grains, designated by superscripts α and β, from a reference orientation, coincident with the specimen axes, to their present orientations. If the components of these rotations, A_{ij}^{α} and A_{kl}^{β}, are referred to the specimen axes, then rotation of a crystallite, whose axes are referred to configuration α, from configuration α to β is given by

$$A_{ij}^{\alpha\beta} = \sum_{k=1}^{3} A_{ki}^{\alpha} A_{kj}^{\beta}. \tag{29}$$

By writing the rotation as viewed from the crystal axes, the axes of the Rodrigues space coincide with the crystal axes. Since the relative orientation of α as viewed from the coordinate system of configuration β is the transpose of (29), the components of the Rodrigues vector for one rotation are the negative of the components of the vector for the other. Thus, since which grain is taken

as reference is arbitrary, distributions of grain misorientations may be represented in half of the subspace. This representation of near neighbor misorientation is shown in Figure 9b. For this particular specimen, the points are clustered more heavily near the center, implying that the neighboring grains tend to have similar orientations.

REMARKS

One of the attractive features of the Rodrigues space representation is that the Rodrigues vectors reside in a rectangular Cartesian coordinate system in which the axes of the space can be chosen to coincide with the specimen axes, and labelled accordingly. The rotations vectors (and the Rodrigues vectors) are determined by the grain orientation and specification of a reference orientation and, therefore, are fixed with respect to the specimen. It follows that (unlike the Euler angle representation) the representation in Rodrigues space rotates with the specimen and does not depend on an established convention that treats each axis differently. Axes of the Rodrigues space coincide with the axes of the refererence orientation and can be used to identify important directions for the specimen.

As illustrated above, crystal orientations plotted in Rodrigues space can show symmetry or asymmetry in a specimen. This is a useful feature for illustrating property variation within a product. Identification of symmetries about 3 orthogonal axes is more difficult in the Euler angle representation.

With more emphasis being placed on effects of neighboring grain interactions, the Rodrigues space representation could be utilized to characterize relative orientations of neighboring grains. Similarly, it also could be used in recrystalization studies where attention is focussed on prior grain orientation and identification of which grain orientations are more likely to consume others during grain growth.

The Rodrigues parameters provide a conceptually simple, physically based method of representing orientation distributions. However, because of the difficulty in imagining objects in three dimensional space, visualizing something as straightforward as rotation of a cube about an axis is not easily accomplished. Analysis

of orientation distributions will still require comparisons with calculated standards to determine crystal orientations in much the same way that CODFs are analyzed.

Determination of the Rodrigues vectors directly from X-rays remains a major obstacle. Presently, the only method available for determining the parameters from pole figure data is by first determining the Euler angles, and converting. In this regard, numerical inversion in the spirit of the "vector" method for Euler angles, or some technique utilizing the pole figure rotation with the Caley–Klein parameters, Eq. (13), may prove useful. Determination of the parameters is not a problem when using the Kikuchi pattern method (Venables and Harland, 1973; Dingley, 1987), but the process is long and tedious, even with much of the process automated. The Rodrigues space does, however, offer advantages over the CODF in terms of Euler angles.

Acknowledgments

The authors would like to thank John Liu of Alcoa Laboratories for providing the grain orientations measured from Kikuchi patterns. We would also like to acknowledge Carol George and Carol Smathers for their help in plotting pole figures and contour plots.

References

Altmann, S. L. (1986). *Rotations, Quaternions and Double Groups*, Oxford University Press, Oxford, U.K.

Asaro, R. J. and Needleman, A. (1985). "Texture Development and Strain Hardening in Rate Dependent Polycrystals," *Acta Metall.* **33,** 923.

Dingley, D. J. (1987). "On-line Micro Texture Determination in a Scanning Electron Microscope" Presented at the 8th International Conference on Texture of Materials, Santa Fe, NM.

Euler, L. (1775). "Formulae generales pro translatione quacunque corporum rigidorum," *Novi Comm. Acad. Sci. Imp. Petrop.* **20,** 189.

Frank, C. F. (1986). "Orientation Mapping," *Polymer NDE,* Proceedings of the European Workshop on NDE of Polymers and Polymer Matrix Composites, Sept. 4–5, 1984 at Termor do Vimeiro, Portugal (ed. K. H. G. Ashbee), Technomic Publishing, Lancaster, PA., 178

Fricke, W. G. and Przystupa, M. A. (1988). "Texture—Components and Their Mechanical Consequences," To be Published in "Modern Aluminum Alloys," ed. A. K. Vasudevan, Academic Press.

Hansen, J., Pospiech, J. and Lücke, K. (1978). "Tables for Texture Analysis of Cubic Crystals," Springer, Berlin.

Hirsch, J., Nes, E. and Lücke, K. (1987). "Rolling and Recrystallization Textures in Directionally Solidified Aluminum," *Acta Metall.* **35,** 427.

Korn, G. A. and Korn, T. M. (1968). *Mathematical Handbook for Scientists and Engineers,* 2nd ed., McGraw-Hill, New York.

Rodrigues, O. (1840). "Des lois géométriques qui régissent les déplacements d'un système solide dans l'espace, et de la variation des coordonnées provenant de ses déplacements considérés indépendamment des causes qui peuvent les produire," *J. de Mathématiques Pures et Appliquées* **5,** 380.

Roe, R. J. (1965). "Description of Crystallite Orientation in Polycrystalline Materials. General Solution to Pole Figure Inversion," *J. Appl. Phys.* **36,** 2024.

Venables, J. A. and Harland, C. J. (1973). "Electron Backscattering Patterns in Scanning Electron Microscopy," Inst. of Phys. Conf. Series No. 18, Inst. of Phys., Bristol and London, 294.